Journal of Power Sources 195 (2010) 6559–6569

Contents lists available at ScienceDirect

Journal of Power Sources

journal homepage: www.elsevier.com/locate/jpowsour

# A sizing-design methodology for hybrid fuel cell power systems and its application to an unmanned underwater vehicle

Q. Cai [a], D.J.L. Brett [a], D. Browning [b], N.P. Brandon [a,*]

[a] Department of Earth Science and Engineering, Imperial College London, London SW7 2AZ, UK
[b] Physical Sciences Department, DSTL, SP4 0JQ, UK

ARTICLE INFO

*Article history:*
Received 29 January 2010
Received in revised form 14 April 2010
Accepted 25 April 2010
Available online 15 May 2010

*Keywords:*
Hybrid fuel cell power system
Sizing-design methodology
Unmanned underwater vehicles

ABSTRACT

Hybridizing a fuel cell with an energy storage unit (battery or supercapacitor) combines the advantages of each device to deliver a system with high efficiency, low emissions, and extended operation compared to a purely fuel cell or battery/supercapacitor system. However, the benefits of such a system can only be realised if the system is properly designed and sized, based on the technologies available and the application involved. In this work we present a sizing-design methodology for hybridisation of a fuel cell with a battery or supercapacitor for applications with a cyclic load profile with two discrete power levels. As an example of the method's application, the design process for selecting the energy storage technology, sizing it for the application, and determining the fuel load/range limitations, is given for an unmanned underwater vehicle (UUV). A system level mass and energy balance shows that hydrogen and oxygen storage systems dominate the mass and volume of the energy system and consequently dictate the size and maximum mission duration of a UUV.



## 1. Introduction

The advantages of hybridizing fuel cells with other energy storage units, such as batteries and supercapacitors, are well known [1,2]. Using the fuel cell and chemical fuel store as the primary energy generator, whilst using a battery/supercapacitor as an energy buffer, can reduce the burden of each single device in supplying the power demand over the entire power cycle for many applications. This is particularly the case for applications that involve dynamic load changes where peak power is only required for some of the time. Such an approach often allows the energy units to be downsized, which lowers the capital cost, reduces physical size and results in improved system efficiency and thus longer operating periods between refuelling. These advantages have prompted investigations into hybrid fuel cell systems as power sources for a variety of road vehicles [3–10], air vehicles [11,12] and underwater vehicles [13]; as well as for distributed power generation in residential areas [14] and for portable, back-up and emergency applications [15–18].

Design of hybrid fuel cell power systems relies on a thorough understanding of how fuel cells and energy storage devices operate, as well as the integration of the two. Electrical integration of the system, i.e. the power sharing between the fuel cell and its associated energy storage unit, is one of the key aspects when designing effective hybrid fuel cell systems. Efforts have been made to investigate different electrical control strategies. These control strategies variably aim to maximise fuel cell power [19], fuel cell efficiency [19] and system efficiency [4], and/or minimise fuel consumption [7,9]. Whilst most of these studies give their attention to the electrical integration and performance of the hybrid system (which are certainly important), in this paper we focus on the selection and sizing of hybrid power units and chemical energy storage.

We present a methodology (hereafter referred to as the 'sizing-design' method) that can be used to inform hybrid system design decisions in order to meet the power and energy demand for a given application, while at the same time meeting the weight and volume constraints. In addition, we also briefly review some of the power source and chemical storage technologies available and how they suit different applications.

Fig. 1 gives a simple illustration of a generic hybrid fuel cell power system, which shows the main components, i.e. the fuel cell system, which consists of a fuel cell stack, fuel supply, oxidant supply, auxiliaries such as fans and pumps and for certain systems a fuel and/or oxidant processor stage; the energy storage system, which may consist of a battery, supercapacitor, or the combination of the two; and the electronic regulation system, which controls the flow of electrical power between the fuel cell, energy storage system and the application load. It should be noted that heat is also generated by the fuel cell, but this is not considered as a useful commodity

* Corresponding author. Tel.: +44 20 7594 5704; fax: +44 20 7594 7444.
*E-mail address:* n.brandon@imperial.ac.uk (N.P. Brandon).

0378-7753/$ – see front matter © 2010 Elsevier B.V. All rights reserved.
doi:10.1016/j.jpowsour.2010.04.078

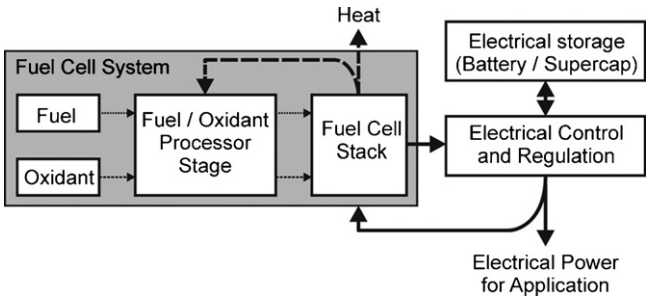


**Fig. 1.** A schematic illustration of the fuel cell hybrid power system.

in this analysis and will need to be dissipated to the surrounding environment.

The sizing-design methodology presented here is ideally suited to applications with a relatively simple power profile composed of discrete power levels repeated on a cyclic basis. Such load demand profiles are common for many applications, including, for example, certain remote communications stations and portable electronic devices. Here, we will use the example of an unmanned underwater vehicle (UUV) to show how the method can be applied.

## 2. The sizing-design methodology

Fig. 2 shows a flow diagram that illustrates the sizing-design method for a hybrid fuel cell power system. The following sections describe each step of the process.

### 2.1. Description of the sizing-design methodology

#### 2.1.1. The application and power cycle

The methodology described is intended for applications where the power demand is known *a priori* (or can at least be approximately predicted), and the power profile exhibits a two-level cyclic characteristic. The power will be distributed between the energy units such that the fuel cell will supply a constant average power (as this will increase the lifetime of the fuel cell and means that it can be designed to have optimum efficiency for a set operating point) and the energy storage unit will supply the peak power and be recharged by the fuel cell during the low power demand periods.

In addition to the power profile, the application is also likely to have constraints on the volume and mass available to the power conversion technology and fuel/oxidant supply systems, as well as the type of fuel to be used. For some applications, very specific environmental constraints exist as shown later for the example of an unmanned underwater vehicle (UUV).

#### 2.1.2. Non-dimensional parametric characterisation

The hybridisation of a fuel cell and electrical energy storage unit depends on the system power requirement. To characterize this, it is useful to define a variable called the 'degree of hybridisation' (*DOH*) as follows [6]:

$$DOH = \frac{\text{maximum power} - \text{fuel cell power}}{\text{maximum power}} \quad (1)$$

where the power from the electrical energy storage unit is equal to the maximum power minus the fuel cell power. As defined in Eq. (1), a low *DOH* value indicates a relatively low power output from the energy storage unit compared to the fuel cell; whilst a high *DOH* indicates a relatively high power output from the energy storage unit. When a battery is used as the energy storage unit, Eq. (1) can be written as [20]:

$$DOH = \frac{\text{battery power}}{\text{battery power} + \text{fuel cell power}} \quad (2)$$

Fig. 3 shows a generic power profile used in this analysis. It is composed of cyclic periods of high and low power requirement, both of variable time; the hybridisation of the fuel cell and battery/supercapacitor intends the fuel cell to supply the constant average power, and the battery/supercapacitor the peak power. The energy storage device is then recharged during the period when the delivered power to the load is below the average power.

If we define $T$ as the ratio of the discharge time $t_1$ to the recharge time $t_2$, Eq. (3), and $F$ as the ratio of the peak power $P_1$ to the base power $P_2$, Eq. (4), and note that the average power ($P_{\text{average}}$) is given by Eq. (5), the degree of hybridisation can be represented as a function of $T$ and $F$, as shown in Eq. (6).

$$T = \frac{t_1}{t_2} \quad (3)$$

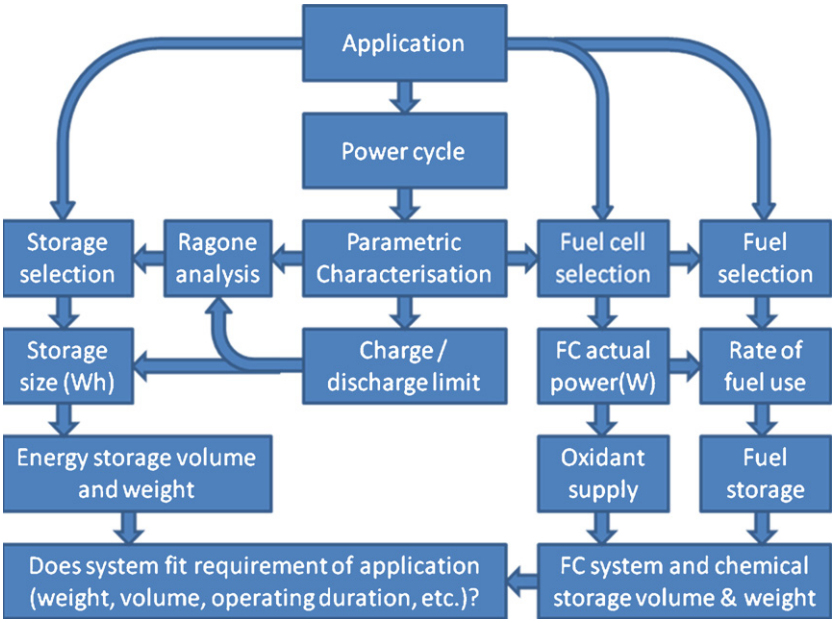


**Fig. 2.** Flow diagram summarising the sizing-design methodology.

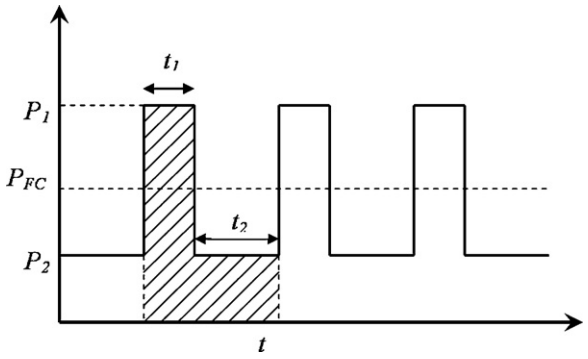


**Fig. 3.** A generic power profile.

$$F = \frac{P_1}{P_2} \quad P_1 \geq P_2 \quad F \geq 1 \tag{4}$$

$$P_{\text{average}} = \frac{P_1 t_1 + P_2 t_2}{t_1 + t_2} \tag{5}$$

$$DOH = \frac{P_1 - P_{\text{average}}}{P_1} = \frac{F - 1}{F(T + 1)} \tag{6}$$

There are several benefits to using non-dimensional parameters to describe load profiles. These include: (i) in certain circumstances scale is not important and it is the type of technology and combination (hybridisation) of technologies that is critical; (ii) specific applications can be described generically by describing them with simple parameters; (iii) simple parameters make numerical analysis and system optimisation easier; and (iv) it is possible to graphically represent or 'map' technology types/combinations onto application requirements. Multi-objective optimisation of hybrid systems employing non-dimensional parameters will be the subject of a future publication.

Fig. 4 shows a contour plot that relates the power profiles, described in terms of *F* and *T*, to the *DOH*. Graphical representations have been added at various regions to show how the characteristics of the load profile vary across the range of possible load profiles. This representation is intended to act as a load cycle characterisation map to aid selection of the right combination of technologies at the appropriate size for hybridisation.

The 'map' shows that as *F* increases, *DOH* increases. The increase of *F* means that the peak power $P_1$ is increasing relative to the base load power $P_2$, as indicated by Eq. (4). The increase of *DOH* with *F* becomes more prominent in the region of very small *T*, *i.e.* *DOH* has a dramatic increase with decreasing *T*. The decrease of *T* indicates that the load power duration, $t_2$, is becoming longer relative to the peak power duration, $t_1$. From the above observation, we conclude that a high *DOH* is found with a power profile characterized by a large gap between the peak power demand and the base load power, and a short discharge time of the peak power and a relatively long base load time interval.

The power profiles illustrated at the top of Fig. 4 are characterized by large *F* (i.e. $10^3$), which means the peak power is 1000 times the base power, whilst power profiles towards the bottom of the chart tend to a constant power demand. As *T* increases from $10^{-3}$ to $10^3$ (from left to right on the figure), the *DOH* value decreases. In this we see that when the energy storage unit's discharge period is much shorter than its recharge period (e.g. the power profiles on the left), the energy storage acts as the major power supply, whilst when the energy storage unit's discharge period is much longer than its recharge period (e.g. the power profiles on the right), the fuel cell contributes as the major power supply.

For a power profile such as that in Fig. 3, the energy discharged from the energy storage unit is

$$E_S = n(P_1 - P_{\text{average}})t_1 \tag{7}$$

and the energy from the fuel cell is

$$E_{FC} = P_{FC}(t_1 + t_2)n = P_{FC}t_{\text{total}} \tag{8}$$

where *n* is the number of cycles, which indicates the total length of the operation period. $P_{FC}$ would be equal to $P_{\text{average}}$ if fuel cell is only to supply the average power as indicated in Fig. 3. If fuel cell is to supply the average power as well as the power required

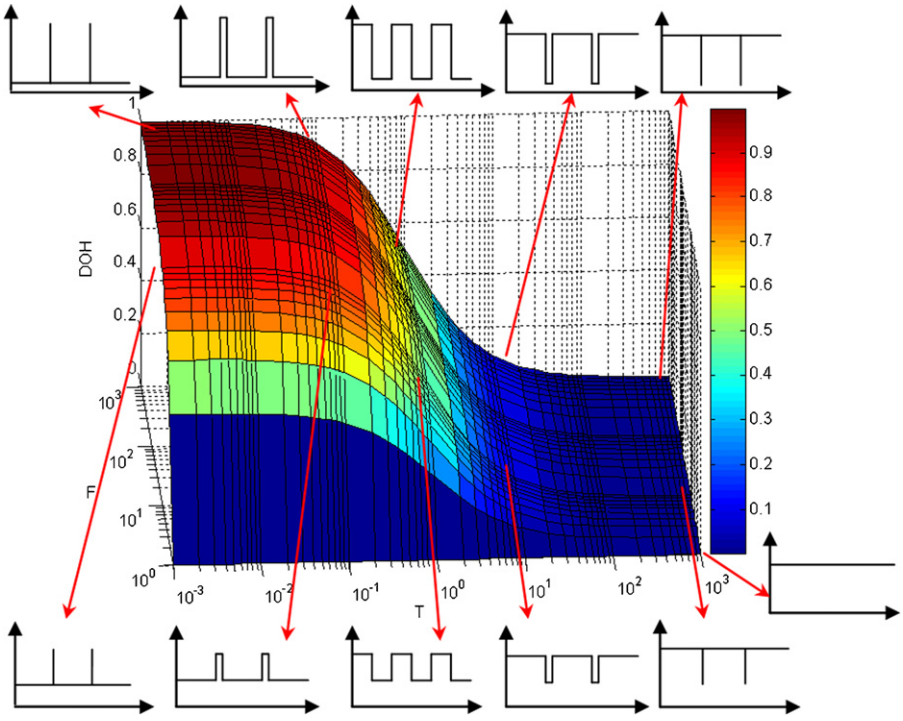


**Fig. 4.** A parameter map in terms of *T*, *F* and *DOH*, describing a wide range of possible power cycle profiles.

from the balance-of-plant auxiliary units such as pumps and fans that are necessary to support the fuel cell system, $P_{FC}$ would be equal to $P_{average}$ plus the power required from the auxiliaries. The latter case will be relevant in Section 3 where the sizing-design methodology is applied to a practical application. In any case, it is the average power that is directly linked to charging the energy storage unit. The parameters $E_S$ and $E_{FC}$ are used to estimate the size of the energy storage unit and the fuel cell system for a given application.

*2.1.3. Charge/discharge limitation (characteristic time)*

Depending on the nature of the power profile, either the charge or discharge process will be the fastest. It is important to establish which is fastest in order to identify the storage technology that is capable of achieving the required charge/discharge rate, and to establish the efficiency of the process at that particular rate.

Given that:

$$P_{average} > P_2 + \frac{1}{2}(P_1 - P_2) \quad \text{charge limited} \tag{9}$$

$$P_{average} < P_2 + \frac{1}{2}(P_1 - P_2) \quad \text{discharge limited} \tag{10}$$

It can be shown that for given $T$ and $F$ values, if the DOH is less than the expression in Eq. (11), the system is charge limited, and below it, Eq. (12), discharge limited.

$$DOH < \frac{2T(F-1)}{F(T+1)^2} \quad \text{charge limited} \tag{11}$$

$$DOH > \frac{2T(F-1)}{F(T+1)^2} \quad \text{discharge limited} \tag{12}$$

Fig. 5 shows the boundary between the two domains, i.e. when the DOH is equal to

$$DOH = \frac{2T(F-1)}{F(T+1)^2} \tag{13}$$

Once the limiting process (charge or discharge) has been determined, the time taken for the limiting process, referred to as the *characteristic time*, can be calculated. This is either $t_1$ or $t_2$. This is then used in the Ragone analysis, described in the next section, for the selection of the storage technology.

## 2.2. Technology selection

*2.2.1. Energy storage technologies and Ragone analysis*

The choice of the candidate energy storage device depends on its characteristics and the requirement of the power to be drawn from it. For example, if there is a demand to supply high power within the time scale of seconds, a supercapacitor may be a better choice than a battery; whilst an advanced battery is able to store more energy in the same weight/volume and thus supports longer peak load. Some workers have combined the two technologies to take advantage of their relevant merits [21,22].

At present, candidate energy storage systems for hybrid fuel cell vehicle applications include the valve-regulated lead-acid (VRLA) battery, nickel–cadmium (Ni–Cd) battery, nickel-metal hydride (NiMH) battery, lithium-ion battery, sodium–nickel chloride (ZEBRA) battery and supercapacitor. Table 1 lists the characteristics of these batteries and supercapacitors. The choice of battery/supercapacitor is made according to the power and energy requirement of the vehicle, as well as cost and compatibility with the application environment.

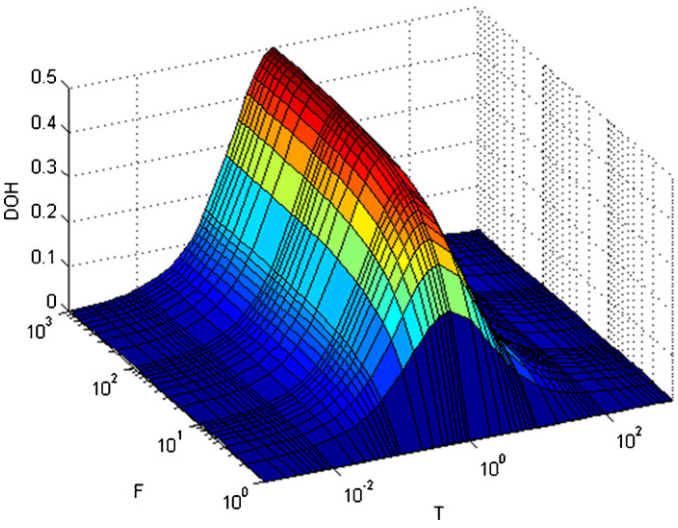


**Fig. 5.** Graph showing the boundary between charge limited (below the surface) and discharge limited (above the surface) performance for DOH as a function of the dimensionless parameters $F$ and $T$.

An appreciation of the relevant features and charge/discharge characteristics is important when matching the technology to the application. Further details can be found elsewhere [22,27–29]. The energy required to be stored in a battery pack needs to be estimated by taking into account the efficiency of the battery and the discharge limit. The efficiency of the battery or supercapacitor is a function of the charge/discharge rate and the state of charge. It is not conducive to a battery or supercapacitor's long-term performance to be fully discharged [30]. Hence in practice a lower limit is set below which a battery or supercapacitor should not be discharged.

When comparing different electrical energy storage technologies, it is often useful to contrast the energy density against the power density in the form of a Ragone plot, as shown in Fig. 6. The domains for each technology type shown on the plot are intended as a guide to indicate where different technologies reside. Rapid advancements, particularly in the area of Li batteries, are causing Ragone plots to be constantly redrawn. The technologies have a spectrum of performance, from the top left hand corner (high energy storage, low power density) to the bottom right hand corner (low energy density, high discharge rate/power density). No single technology has both very high power and energy density, this is part of the reason for the need for hybridisation - note that both axes are shown on a logarithmic scale.

**Table 1**
Comparison of different energy storage technologies.

| | Lead-acid [23] | Ni–Cd [24] | NiMH [25] | Li-ion [26] | ZEBRA [24] | Supercapacitor [23] |
|---|---|---|---|---|---|---|
| Specific energy (Wh kg$^{-1}$) | 35 | 45 | 65 | 100 | 120 | 1–10 |
| Energy density (Wh L$^{-1}$) | 120 | 110 | 135 | 115 | 140 | N/A |
| Specific power (W kg$^{-1}$) | 100 | 120 | 1000 | 1800 | 180 | (1–10) 000 |
| Self-discharge per month (%) | 8 | 10 | 30 | 5 | None | 50 |
| Nameplate cycle life | 1000 | 1000 | 1000 | >2000 | 2000 | 100,000 |
| Efficiency (%) | 70 | 80 | 80 | 85 | 90 | 95 |
| Operation temperature (°C) | −15–45 | −40–70 | −30–70 | −20–60 | 275–350 | −40–50 |
| Cost (£ kW h$^{-1}$) | 105–175 | 200–300 | 250–350 | 250–1000 | 70–270 | 10,000 |

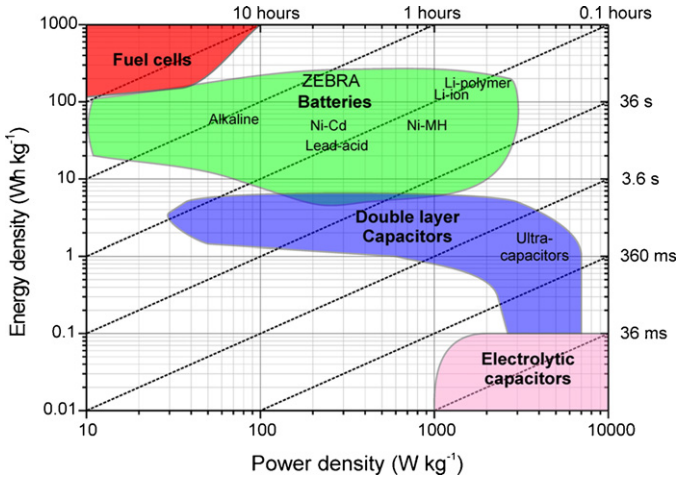


**Fig. 6.** Ragone plot describing energy storage technologies in terms of energy density and power density. Diagonal perforated lines represent different characteristic times.

To use this plot to inform energy storage technology selection (or at least discount certain technologies) we first need to use the characteristic time, determined in Section 2.1.3, i.e. the maximum period of time over which the electrical storage system needs to deliver maximum power. Using this value, a diagonal line can be drawn across the Ragone plot. The storage technology with the lowest overall mass will lie on this line and as far to the top-right as possible.

In practice, it is unlikely that any given technology will sit directly on the characteristic time line; by moving away from the line either the power or energy available from the system will be oversized. We must therefore decide whether the power delivery or energy storage requirement will lead to a larger (i.e. heavier) system. Of course, it is possible for any of these technologies to satisfy a given power/energy requirement if made large enough, but the purpose of this analysis is to identify the lowest mass system. An equivalent analysis can also be performed on a volumetric basis; however, for electrochemical energy storage devices it is usually the mass that is the limiting factor.

We therefore need to decide if it is preferable for the energy or power of the system to be oversized. For example, for an application requiring a relatively high power requirement compared to energy requirement it is better to select a technology with a higher gravimetric power density and oversize the energy capacity, since this will result in a lower overall system mass.

Once a clear impression of the range of possible electrical storage technologies is available form the Ragone analysis, detailed consideration of the specific performance characteristics of each can take place. Factors specific to the application must be considered, such as the impact of efficiency on the limiting charge/discharge rate. When calculating the name plate energy capacity of the device, the efficiency of the limiting process and the discharge limit need to be considered, as shown in Eq. (14).

$$\text{name plate energy capacity} = \text{energy consumed} \times \frac{1}{\text{efficiency}} \times \frac{1}{\text{discharge limit}} \quad (14)$$

A typical battery efficiency is of the order of 0.7 (for lead acid batteries)–0.9 (for lithium batteries), and the discharge limit around 80% of full discharge [30,31] (these values will typically be higher for supercapacitors). However, this will depend on the rate of discharge/charge required.

The weight and volume of a battery or supercapacitor system (termed as $W_S$ and $V_S$ respectively) capable of storing this energy (expressed as Wh) is calculated using the gravimetric energy density (Wh kg$^{-1}$) and volumetric energy density (Wh L$^{-1}$), as given in Eqs. (15) and (16).

$$W_S = \frac{\text{name plate energy capacity}}{\text{specific energy of a battery or supercapacitor}} \quad (15)$$

$$V_S = \frac{\text{name plate energy capacity}}{\text{energy density of a battery or supercapacitor}} \quad (16)$$

It is important to realise that this analysis is designed to exactly fit the needs of the application; in practice, judicious over-sizing of the system is necessary to account for off-design operation and loss in performance over time.

### 2.2.2. Fuel cell technology selection

Various fuel cell technologies exist, each with their own characteristics such as operating temperature and materials of construction. The choice of an appropriate fuel cell technology depends on the requirements of the application [1,32]. Table 2 compares the main types of fuel cell technology that have been used for mobile applications; namely, the polymer electrolyte fuel cell (PEFC), intermediate temperature solid oxide fuel cell (IT-SOFC) and alkaline fuel cell (AFC).

The low temperature operation of PEFCs affords quick start-up, making them well suited to transportation applications that involve frequent on and off operations. Hybrid PEFC power systems have been studied for use in cars [7,33–36], city buses [8], scooters [37], airplanes [11], and underwater vehicles [13]. They have also been seen used in portable applications [17] and intelligent uninterruptible power supply systems [18]. SOFCs are mainly used for stationary applications where heat can be utilised. In recent studies, intermediate temperature SOFCs (IT-SOFCs) [38] hybridised with

**Table 2**
Comparison of three fuel cell technologies.

| | PEFC | IT-SOFC | AFC |
|---|---|---|---|
| Cell materials | Electrode: Pt/C<br>Electrolyte: polymer membrane<br>GDL: carbon materials | Electrode: ceramic materials<br>Electrolyte: ceramic materials | Electrode: Pt/C<br>Electrolyte: KOH solution<br>Nickel mesh support |
| Fuel | Hydrogen (high purity, no CO) | Hydrogen (with low CO)<br>Hydrocarbons | Hydrogen (high purity, free of $CO_2$) |
| Oxidant | Air or pure oxygen | Air or pure oxygen | Air or pure oxygen (free of $CO_2$) |
| Operating temperature | <80 °C | 500–800 °C | 60–100 °C |
| Cooling | Water or air cooling | Air cooling | Circulating electrolyte |
| Advantages | Well developed<br>Quick start-up | Well developed<br>Wide choice of fuels | High efficiency<br>Low cost |
| Disadvantages | Expensive<br>Water management can be a problem | Long start-up time<br>Low volumetric power density | Severe problems with $CO_2$ |

**Table 3**
Hydrogen storage methods. The gravimetric density $\rho_m$, the volumetric density $\rho_v$, the working temperature $T$ and pressure $P$. RT refers to room temperature.

| Storage method | $\rho_{mH_2}$ (kg $H_2$ kg$^{-1}$) | $\rho_{vH_2}$ (kg $H_2$ m$^{-3}$) | $T$ (°C) | $P$ (bar) | Remarks |
|---|---|---|---|---|---|
| High pressure gas cylinders [13] | 0.012 | 16 | RT | 200 | Compressed gas, in steel, or light weight composite cylinders |
| | 0.032 | 21 | RT | 350 | |
| | 0.06 | 35 | RT | 700 | |
| Liquid hydrogen in cryogenic tanks [47] | 0.142 | 70.8 | −253 | 1 | Continuous loss of a few wt% per day of hydrogen at RT |
| Adsorbed hydrogen [47,48] | ~0.02 | 20 | −80 | 100 | Present performance |
| | 0.071 | 29.6 | −80 | 100 | US DOE target |
| Absorbed on interstitial sites in host metals FeTi, $LaNi_5$ | ~0.02 | 115 | RT | 1 | Refuelling pressure about or above 100 bar |
| $BH_3NH_3$ [49] | 0.11 | 115 | >RT | 1 | Under development |

ZEBRA batteries have been considered as power sources for road vehicles [24,39,40] and hybridised with gas turbines for unmanned air vehicles [12]. Micro-CHP at the residential scale is also an ideal application for this class of fuel cell [41]. Alkaline fuel cells have been trialled extensively in vehicular systems [42], including space missions.

### 2.2.3. Fuel selection and storage of hydrogen

The power capability of the fuel cell stack can be varied independently of the energy storage capability. When a high energy storage density is required, it is the properties of the fuel and oxidant sub-systems that dominate the overall size of the complete fuel cell plant. Applications in the transportation sector require storage at a volume that can be accommodated within vehicles, and at a weight that does not limit vehicle performance. Also, for building integrated applications, storage volume must usually be restricted. It is thus very important to carefully choose the fuel and fuel storage technologies to fit the system requirements.

In this work, we will concentrate on hydrogen as the fuel for the fuel cell and compare several commercially available and potentially available hydrogen storage methods, as summarised in Table 3. It should be noted that, although there is a lot of data in the literature about the gravimetric and volumetric density values of hydrogen storage materials, this is not sufficient for engineering design purposes. Hence the gravimetric and volumetric density values of the hydrogen storage techniques given in Table 3 have been estimated for the whole storage system, which includes the tank, valves, and other balance-of-plant. Each of these hydrogen storage techniques has its advantages and disadvantages, and the choice of the hydrogen storage technique depends on the application. In this study, energy storage capacity is of primary concern. The volumetric density of compressed or liquid hydrogen, as well as the gravimetric density of hydrogen stored in metal hydrides, is considered too low for transportation applications. Many researchers see chemical hydrides as a more viable alternative. Amongst such hydrides, sodium borohydride, lithium amide and magnesium hydride [43–46] have been largely studied whereas satisfactory storage capacity has not been achieved. We do not consider these hydrides here since reliable estimates of the system-based storage capacity are not available in the literature. Ammonia borane ($NH_3BH_3$) [49] is considered to be a promising hydrogen storage material, largely on account of its relative safety and high hydrogen content (19.6 wt%, 0.145 kg $L^{-1}$ $H_2$). This storage technique is still under development and researchers recognize that there are real improvement opportunities for hydrogen releasing processes from $NH_3BH_3$. In this paper, an estimation of the gravimetric density (0.11 kg $H_2$ kg$^{-1}$ $NH_3BH_3$) and volumetric density (115 kg $H_2$ m$^{-3}$ $NH_3BH_3$) is used, assuming continuing progress is made with this approach.

The graph shown in Fig. 7 can be used to help select the optimum hydrogen storage technology on a volume or mass basis. The chart allows any one of the following parameters to be found with knowledge of the rest: mass/volume, technology type, fuel consumption rate for a given applications and time between refuelling. For example, given a certain technology, the chart allows the designer to trade-off fuel consumption rate with operating time between refuelling (or range in the case of a transport application) for a given mass or volume constraint; or determine which storage technolo-

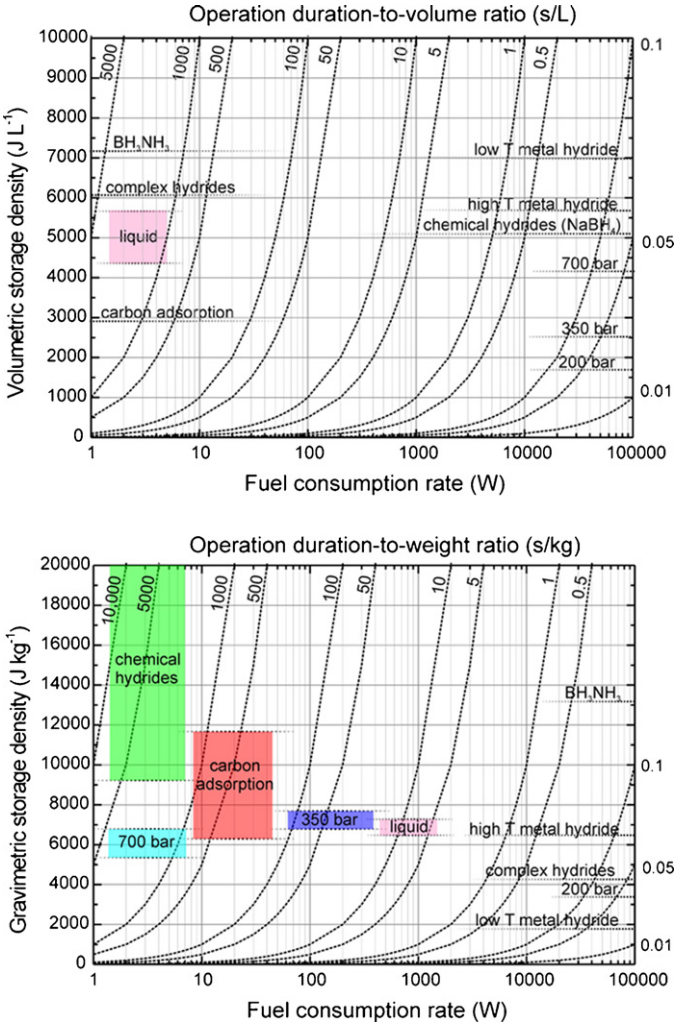


**Fig. 7.** Hydrogen storage technology selection charts based on volumetric (top) and gravimetric (bottom) considerations.

**Table 4**
Three oxygen storage methods. The gravimetric density $\rho_m$, the volumetric density $\rho_v$, the working temperature $T$ and pressure $P$. RT refers to room temperature.

| Storage method | $\rho_{mO_2}$ (kg $O_2$ kg$^{-1}$) | $\rho_{vO_2}$ (kg $O_2$ m$^{-3}$) | $T$ (°C) | $P$ (bar) | Remarks |
|---|---|---|---|---|---|
| Compressed oxygen | 0.213 | 166.7 | RT | 153 | Compressed in light weight aluminium cylinders |
| Liquid oxygen | 0.786 | 661 | −118.6 | 3–55 | Liquefied and stored in cryogenic tanks |
| 70 wt% $H_2O_2$ | 0.303 | 348.8 | 40 | 1 | Hazardous fluid |

gies are possible for a given power requirement and operational duration, etc. The application of Fig. 7 will be explained in more details later in Section 3.2.5.

The amount of hydrogen stored on board can be determined based on the energy supply from the fuel cell, when the overall fuel cell system efficiency, $\eta_{FC}$, is known [33]:

$$\eta_{FC} = \frac{E_{FC}}{HHV_{H_2} n_{H_2}} \tag{17}$$

where $HHV_{H_2}$ is the higher heating value of hydrogen, and $n_{H_2}$ is the moles of hydrogen consumed. $E_{FC}$ is the energy required from the fuel cell, calculated using Eq. (8), and dependant on the power profile. Based on Eq. (17) and the parameters given in Table 3, the weight and volume of the various hydrogen storage technologies to supply the energy required can be estimated respectively as $W_{H_2}$ and $V_{H_2}$, as given in Eqs. (18) and (19).

$$W_{H_2} = \frac{2 \times n_{H_2}}{1000 \times \rho_{mH_2}} = \frac{n_{H_2}}{500 \rho_{mH_2}} \tag{18}$$

$$V_{H_2} = \frac{W_{H_2}}{\rho_{VH_2}} \tag{19}$$

*2.2.4. Selection of oxidant supply*

There are a wide variety of ways to supply oxygen to fuel cells. The sources of oxygen in general include: (1) compressed air by using a compressor; (2) pure oxygen storage as a liquid (i.e. liquid oxygen in cryogenic cylinders) or gas (i.e. compressed oxygen in high pressure tanks); (3) released from oxygen-rich compounds, such as hydrogen peroxide ($H_2O_2$) and sodium chlorate; (4) extraction from water by electrolysis together with membrane separation, if the electricity required for this process is from another energy source such a battery, or separate generator.

Using an air compressor/blower is the most commonly used method to supply oxygen to fuel cells. There are, however, some circumstances where air is not available (for example, in air-independent underwater vehicles, as will be described in Section 3) and so oxygen must be stored onboard. Also, compressors are very energy-consuming, the compressor power can consume up to 30% of the fuel cell stack power, contributing up to 93.5% of the total auxiliary power consumption [9]. There are advantages of using pure oxygen; it leads to a performance increase in the output voltage of the fuel cells, compared to operation on air at given conditions [33], and it avoids the power required for the air compressor.

Table 4 gives the gravimetric and volumetric density of three oxygen storage methods that supply pure oxygen: compressed, liquid and $H_2O_2$. Note that these are estimates based on the whole storage system which includes containers and valves, etc. The weight and volume of the various oxygen storage technologies can be estimated respectively as $W_{O_2}$ and $V_{O_2}$, by relating to the gravimetric density ($\rho_{mO_2}$) and the volumetric density ($\rho_{vO_2}$) of the oxygen storage system, as given in Eqs. (20) and (21).

$$W_{O_2} = \frac{(n_{H_2}/2) \times 32}{1000 \times \rho_{mO_2}} = \frac{0.16 n_{H_2}}{\rho_{mO_2}} \tag{20}$$

$$V_{O_2} = \frac{W_{O_2}}{\rho_{VO_2}} \tag{21}$$

*2.2.5. System integration*

The mass and volume of the hybrid fuel cell power system (i.e. $W_{total}$ and $V_{total}$) can be estimated by summing the fuel cell stack (i.e. $W_{FC}$ and $V_{FC}$), system auxiliaries (i.e. $W_{auxiliaries}$ and $V_{auxiliaries}$), hydrogen supply (i.e. $W_{H_2}$ and $V_{H_2}$), oxygen supply system or storage (i.e. $W_{O_2}$ and $V_{O_2}$) and the energy storage device (i.e. $W_S$ and $V_S$), expressed below as Eqs. (22) and (23).

$$W_{total} = W_{FC} + W_{auxiliaries} + W_{H_2} + W_{O_2} + W_S \tag{22}$$

$$V_{total} = V_{FC} + V_{auxiliaries} + V_{H_2} + V_{O_2} + V_S \tag{23}$$

We have demonstrated in the previous sections that, from a power profile, the estimation of the mass and volume of hydrogen supply, oxygen supply/storage and the energy storage device. The estimation of the mass and volume of the fuel cell stack and system auxiliaries will depend on the system design (e.g. which type of fuel cell is chosen and what would be included in the system auxiliaries) and the products available on the market. This will be better illustrated for a specific fuel cell power system design and for a specific application, as will be shown in Section 3. For the chosen technologies, the estimated size of the hybrid fuel cell system can then be determined. On the other hand, with size constraints imposed (i.e. $W_{total}$ and $V_{total}$ on the left hand of the equation) we can evaluate the viability of different technologies.

## 3. Sizing-design methodology applied to the example of a light-weight unmanned underwater vehicle (UUV)

### 3.1. The power system requirement of UUVs

Underwater vehicles are ideally suited to provide surveillance, remote sensing and communication relay capabilities for both military and civilian applications. Practical examples include oceanographic data gathering, environmental monitoring, mine detecting and coastal defence. The power system of underwater vehicles has long been a major consideration in designing and manufacturing these vehicles for particular missions. This is because the power system usually determines the ultimate performance (e.g. endurance, cruising speed and distance) of an underwater vehicle. Stealth is an important design consideration for many UUV applications as it enables the vehicle to operate anywhere, at any time, without being detected. Besides helping to avoid detection, stealth enhances the vehicle's ability to detect targets by eliminating/reducing self-noise. To meet the stealth requirement, an air independent power (AIP) system is beneficial to underwater vehicles. The ideal AIP source for an underwater vehicle will be quiet, have a low thermal signature, will not discharge anything from the submarine system, and will of course be capable of operating without atmospheric air.

A fuel cell power system is suited for the underwater vehicle as it releases no gaseous emissions and only low-grade noise during operation, when fuelled with hydrogen and oxygen. Different types of fuel cells have been used for the power system in underwater vehicles. For example, the Norwegian Defence Research Establishment and Naval Undersea Warfare Centre in the USA developed 'semi-fuel cells', using aluminium [50] and magnesium [51,52] as the electrodes, alkaline solution as the electrolyte and hydrogen peroxide as the oxidant. The 'semi-fuel cells' consume the metallic anode, so the entire energy system needs to be replaced after

**Table 5**
Parameters for a light-weight UUV.

| | |
|---|---|
| External diameter | 32.4 cm (12.75 in.) |
| Internal diameter | 28.6 cm (11.26 in.) |
| Length | 3.76 m (148 in.) |
| Weight | ~227 kg (500 lbs) |
| Payload | 92.6 kg |
| Operation depth | 200–500 m |
| Energy section | |
| Volume | 24% $V_{total} \approx 58$ L |
| Weight | 24%$V_{total} \times 1025\,kg\,m^{-3} \approx 59$ kg |

each run. These systems provide a high energy density source for low power, long endurance (60 h) applications, but are fairly complex and involve onboard infrastructure and logistics that requires skilled personnel for operation. A direct sodium borohydride fuel cell (DSBFC) has also been studied as the propulsion power [53]. This approach is still under development. The use of SOFCs operating on hydrocarbon fuels has also been proposed for underwater vehicle power systems, together with a reformer and a $CO_2$ capture stage [54,55]. Several papers have addressed the use of PEFCs in UUVs [13,56]. The Japanese submarine Urishima has pioneered the use of a PEFC within an UUV [56]. Griffith et al. [13] modelled the hybrid PEFC system with lithium-ion battery for the UUV using virtual test bed software, focusing on the voltage and current control between fuel cell and battery.

In the following sections, a light-weight UUV will be given as an example to demonstrate our sizing-design methodology. A load cycle will be given and a standard UUV arrangement specified. The design challenge is to determine the best fuel cell power architecture and size as well as determining the mission length based on the most appropriate fuel and oxidant storage technologies for the specific application.

### 3.2. Power system design for a light-weight UUV

#### 3.2.1. Description of a light-weight UUV and its power profile

The details of a light-weight UUV architecture are given in Table 5. This UUV is of a representative torpedo size with an external diameter of 32.4 cm, length of 3.76 m and weight of 227 kg. The UUV has a limited space for the energy section (power conversion and chemical storage section). The energy section is assumed to take up 24% of the UUV's total volume, based on the US MARV demonstrator vehicle which is the same diameter as the UUV used in our analysis but with a longer length of 4.01 m [57]. The neutral buoyancy requirement for the UUV determines the limiting weight of the energy section (which is calculated as the product of the volume and the density of the sea water). Note that when designing a UUV, it is important that the vehicle is neutrally buoyant, i.e. that the mean density of the UUV must equal the density of the surrounding sea water (which has a density of 1025 kg m$^{-3}$). Hence this sets a target density for our complete hybrid system of 1 kg L$^{-1}$.

The power profile for the UUV is given in Fig. 8, which shows periodic high power demand. The high power demand may correspond to the use of the electronic devices for mapping, detection and data collection. The number of activity cycles (shown as solid lines in Fig. 8) determines the mission length of the UUV. The high peak of the propulsive power lasts for 10 min at 6736 W, and the low propulsive power 6.6 h at 210 W. Ideally the mission will last a total of 13 cycles; when the start and finish periods are included, this is equal to a total of 92.35 h. Apart from supplying the propulsive power, the power system in the UUV is also expected to supply the payload power (which may be required for keeping some computer or software running), indicated as the dashed lines in Fig. 8. The calculated total payload energy over the 92.35 h is 8681 Wh.

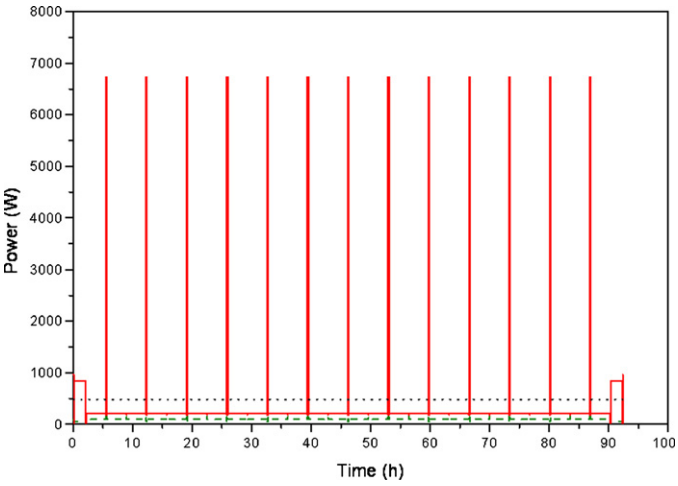


**Fig. 8.** The power profile for a light-weight UUV. Solid lines indicate the propulsive power, dash lines indicate the payload power, and the dotted line indicates the average power.

The average power calculated for the power system is 500 W, which is shown as the dotted line in Fig. 8.

As discussed in Section 2.1, for the power profile shown in Fig. 8, it is appropriate to use a fuel cell to supply the average power, and draw from the energy storage unit (battery or supercapacitor) the power that is equivalent to subtracting the average power from the peak power. Referring to Fig. 4, this power cycle can be expressed in non-dimensional terms as: $T = 0.025$, $F = 32$ and $DOH = 0.928$, indicating that the major portion of the maximum power is going to be drawn from the energy storage unit rather than the fuel cell.

It is worth noting that the power/energy assignment between the fuel cell and the battery would be done through an electrical control and regulation system (as shown in Fig. 1)/a power controller (as will be shown in Fig. 9); thus any inefficiency in the electrical control and regulation system or the power controller would result in an increase in the total energy required from the power system. Although this issue is not discussed quantitatively in this paper, it is clear that a highly effective power controller is desirable, to minimise the extra power demand on the system.

#### 3.2.2. Energy storage selection

Referring to Fig. 5, the *DOH* is well above the boundary and therefore discharge limited and with a characteristic time of $t_1 = 600$ s (i.e. 10 min) in which a total energy of 1039 Wh ($3.74 \times 10^6$ J) needs to be delivered by the energy storage device. Referring to Fig. 6, the diagonal line representing the characteristic time for the system is 0.17 h. This precludes the use of capacitors (including electrolytic, ultra and double-layer capacitors), as well as lead acid batteries, leaving other more advanced battery technologies as the option

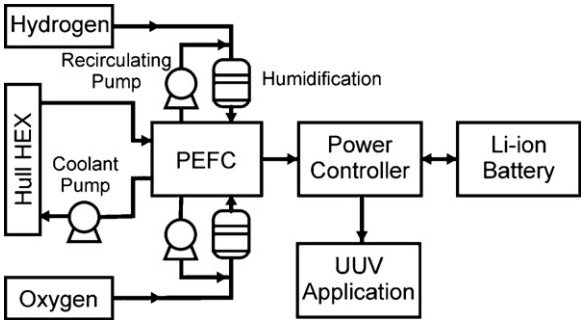


**Fig. 9.** System architecture of the hybrid fuel cell/battery power system for the UUV.

for energy storage, as shown in Fig. 6. On a per kg basis, it is clear that a high power density is more important than a high energy density, since the power and energy requirements are 6236 W and 1039 Wh, respectively. Therefore, if a technology on the characteristic time diagonal line is not available/suitable; the mass of the system will be kept to a minimum by choosing one above the line (high power density) and as far to the right as possible is desirable. In this case, Li technology gives the highest power density; however, we need to consider the allowable mass and volume of the entire system (as given in Table 5) to see what other technologies may be suitable. Therefore, battery technology is the clear choice as the energy storage unit for this application/mission power cycle. The battery, as the dynamic energy storage device, would supply peak and pulse power, and power for start-up of the hybrid system. The fuel cell, as the device that converts the energy from the fuel, supplies the average power (as indicated by the dotted line in Fig. 8) and recharges the battery.

The energy required from the battery is calculated taking into account the efficiency of the battery and the discharge limit using Eq. (14). For the duty cycle shown in Fig. 8, the energy needed to be stored in the battery is 1856 Wh. The weight and volume of the battery system capable of storing this energy is calculated based on available values for the gravimetric and volumetric energy density, as listed in Table 2. On a weight and volume basis, it is clear that Li-ion batteries are optimum. Li-ion battery packs also have the advantage that they can be configured from relatively small cells; thus can be manufactured to fit within most UUV hull shapes. The performance of current Li-ion battery technologies varies significantly between manufacturers. Based on the energy requirement of the system in Fig. 8, SAFT claims to be able to provide the same performance using their VL34P module with a weight of 16 kg and a volume of 9 l. Our estimation of weight and volume based on the Li-ion battery package of 15.4 kg and 8 L is therefore close to the currently commercially available SAFT technology.

### 3.2.3. Fuel cell technology selection

A polymer electrolyte fuel cell (PEFC) is chosen to be hybridised with the Li-ion battery to supply the power for the UUV. The advantage of using a PEFC in our design is that a cooling system using water is enabled (using a section of the hull for heat exchange to the environment), avoiding the need for air. Furthermore, heat transfer using a liquid is far more effective than using a gas, so a low-power pump would therefore be sufficient for driving the coolant flow. In contrast, high temperature fuel cells such as the solid oxide fuel cell (SOFC) operate at temperatures of ~500–1000 °C, and require large amounts of air for cooling and are therefore not suitable for use in an air independent system. In this work, we assume that the PEFC operates at its rated power with an electrical efficiency of $\eta_{FuelCell} = 50\%$, which is in accord with the US DOE target for PEFCs in transportation applications [58].

### 3.2.4. The power system architecture

We propose the power system architecture of the hybrid fuel cell/battery power system for the UUV, as shown in Fig. 9. To cool the PEFC, water is driven through the stack using pumps to transfer the excess heat from the fuel cell to the hull and subsequently to the submarine environment. The hybrid system also includes a constant voltage regulation system, a smart battery charger, and an electricity supply regulation system, which all require careful design but are beyond the scope of this study.

Table 6 gives the power, the estimated mass and volume of the system components, excluding the hydrogen and oxygen storage units. The power required from the fuel cell is set to be the average power (500 W) derived from the power cycle in Fig. 8, plus the power consumed by the auxiliaries such as pumps and fans (estimated to be 100 W), giving a total of 600 W. Based on the PEFC products available from the commercial market, the weight and volume of a 600 W PEFC are estimated to be 5 kg and 7 L, respectively. The total weight and volume of the auxiliaries are estimated to be 6 kg and 6 L respectively. Given that the allowable weight and volume for the entire energy section are 59 kg and 58 L as shown in Table 5, the maximum available weight and volume for the hydrogen and oxygen storage within the UUV are then 33 kg and 37 L.

**Table 6**
Power, mass and volume of system components for the UUV application.

| Component | Power (W) | Mass (kg) | Volume (L) |
|---|---|---|---|
| Fuel Cell | 600 | 5 | 7 |
| Battery | 6240 | 15 | 8 |
| Auxiliary[a] | −100 | 6 | 6 |
| Maximum for hydrogen and oxygen storage | | 33 | 37 |

[a] Pumps, fans, piping, electric controls and cooling radiator.

### 3.2.5. Hydrogen and oxygen storage selection

The UUV application is unusual in that an oxidant as well as fuel needs to be stored.

The $H_2$ store may be in compressed cylinders, in cryogenic cylinders, or in the form of a metal hydride or complex hydride, which can release hydrogen directly. Among the various oxygen storage systems, liquid oxygen storage (LOX) has been previously identified to be the most suitable oxidant for underwater vehicles [55,59]. From Table 4, it is clear that LOX has the highest volumetric and gravimetric density among the commercially available oxygen storage technologies. Advanced light-weight liquid oxygen storage systems have been developed for underwater vehicles by Sierra Lobo Inc. (OH, USA) [13]. However, the storage of LOX raises many safety issues, such as the effects of leakage, boil-off or large shock loads. A full safety/risk assessment is required before LOX is stored on the submarines.

The fuel cell power requirement is 600 W, so taking the electrical efficiency of the fuel cell to be 50%, the fuel consumption rate is equivalent to 1200 W. The amount of oxygen which is needed for the fuel cell operation is estimated by assuming that it reacts completely with the hydrogen used, producing water. Oxygen should be supplied in excess of that which is stoichiometrically required, typically with stoichiometric ratios of 1.2–1.3 (i.e. 20–30% excess), in order to remove product water and ensure that the cathode is not starved of reactant. However, when both hydrogen and oxygen are re-circulated, as in the design model shown in Fig. 9, the reaction ratio of 1.0 mole $O_2$ to 2.0 moles $H_2$ is assumed.

The maximum operation duration-to-volume ratio is calculated to be 9000 s $L^{-1}$ and the maximum operation duration-to-weight ratio 10,077 s $kg^{-1}$, assuming that the power system runs for the full 92.35 h as shown in Fig. 8, and that the hydrogen storage takes the whole volume which is available for both hydrogen and oxygen storage given in Table 6 (of course, this is not the case, but such an assumption is useful in providing a rough idea of the maximum s $L^{-1}$ and s $kg^{-1}$ values). Using Fig. 7, it is clear that none of the hydrogen storage technologies satisfy the volume criteria, as 9000 s $L^{-1}$ is far off of the chart for all the current available hydrogen storage techniques. Although the chemical hydrides, which give the best operation duration-to-weight ratio on the top left corner of the map, might just meet the weight criteria (10,077 s $kg^{-1}$), they do not meet the fuel consumption rate which is 1200 W. Therefore, given a fixed volume for the energy section, the duration of the mission has to be shorter than 92.35 h in order to use current hydrogen storage techniques. This will be further explored in Section 3.3 where a mass and energy balance analysis will explore the envelope of operation duration.

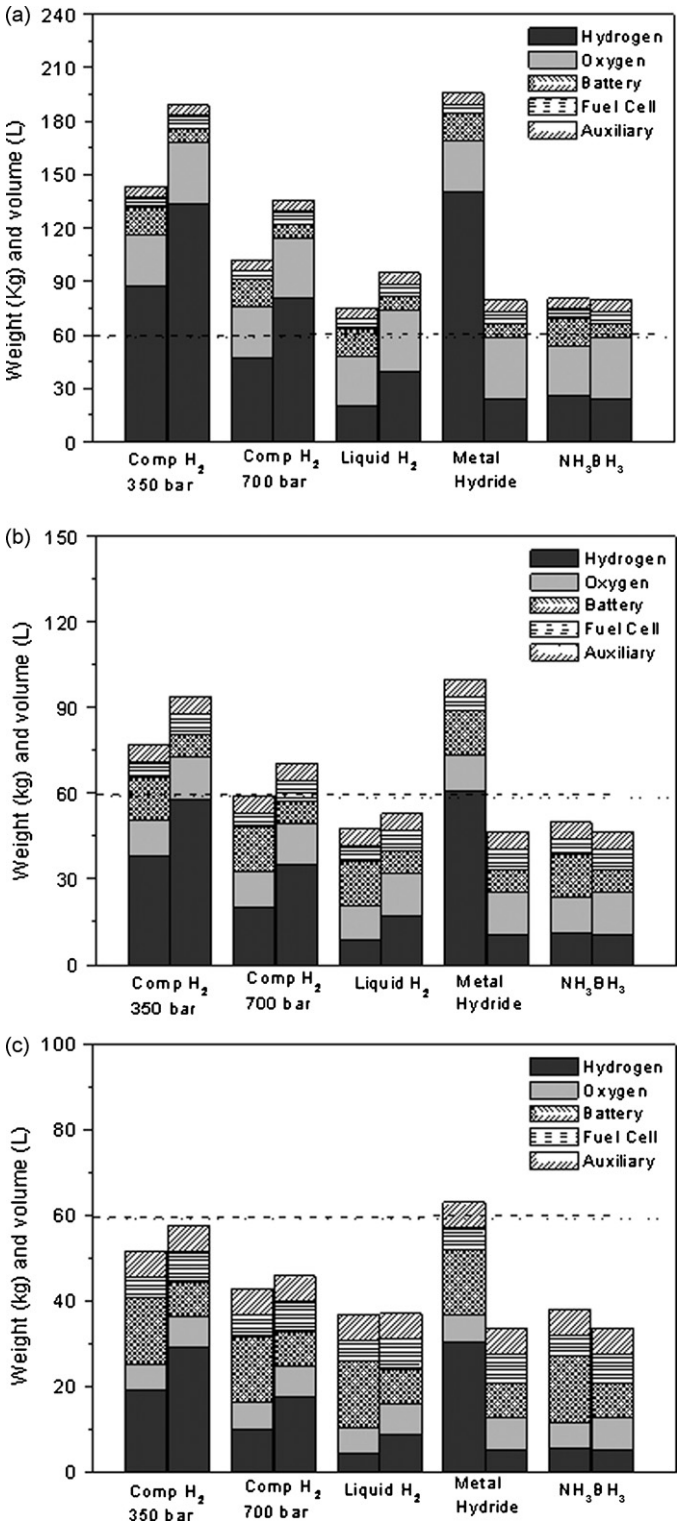


**Fig. 10.** Mass balance analyses for the hybrid fuel cell/battery system assuming it carries out a mission of (a) 92.35, (b) 40, and (c) 20 h. The dashed and dotted lines indicate respectively the maximum allowable weight and volume for the hybrid power system. Several hydrogen storage options are compared. Note that LOX is the chosen oxygen storage technique. The first column is the mass in kg, while the second column is the volume in litre.

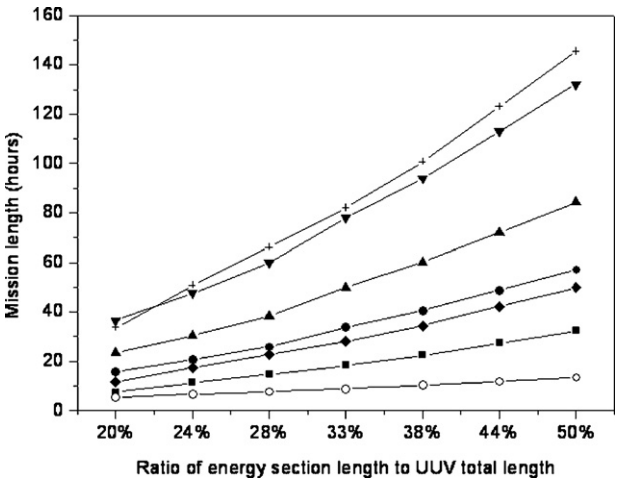


**Fig. 11.** The variation of the mission length with the length of the energy section. The symbol (○) indicates using lithium-ion battery alone to supply power. The other symbols indicate using the hybrid PEFC/Li-ion battery system power system to supply power. LOX is the chosen oxygen storage technique, whilst different hydrogen storage techniques are considered: (■) compressed hydrogen at 20 MPa, (♦) metal hydride, (●) compressed hydrogen at 35 MPa, (▲) compressed hydrogen at 70 MPa, (▼) liquid hydrogen, and (+) $NH_3BH_3$.

### 3.3. Mass and energy balance analysis of the hybrid power system within the UUV

As shown in Table 6, the proposed hybrid power system can fit within the volume and mass requirements of the UUV. But the operation duration will depend on the size of the hydrogen and oxygen tanks that can be fitted within the unused volume. For all the analysis to be discussed in this section, LOX is the chosen oxygen storage technique; whilst several hydrogen storage techniques are examined. If a given element needs to be larger or a new element to be added, then it will be at the expense of reduced hydrogen and oxygen storage capacity, and hence reduced mission length.

Fig. 10 shows the results on the mass balance analysis using Eqs. (17)–(23) for the hybrid fuel cell/battery system, by comparing the different hydrogen storage techniques. The intention is to see how the hydrogen tank, oxygen tank and other components fit in the UUV when the volume of the energy section is fixed as given in Table 5. In Fig. 10(a), the estimates of hydrogen and oxygen are performed by assuming the UUV carries out the mission continuously for 92.35 h, as required in the power profile of Fig. 8. For such a mission length and the given volume capacity, current storage technologies fail to store the required amount of hydrogen and oxygen. As discussed in Section 3.2, the duration of the mission has to be shorter than 92.35 h in order to use current hydrogen storage techniques. Fig. 10(b) and (c) shows the mass balance of the system assuming the lifetime of the UUV mission to be 40 h and 20 h, respectively. At the mission length of 40 h, liquid hydrogen and $NH_3BH_3$, together with oxygen stored in cryogenic tanks, are able to fit within the volumetric and mass constraints of the system. At the mission length of 20 h, hydrogen storage can be chosen from being stored as compressed at 35 or 70 MPa, as liquid and in the form of $NH_3BH_3$.

We then examine how the volumetric and mass requirements of the UUV influence the system design and the lifetime of the mission. This is done by considering how varying the fraction of length (with constant cross-sectional area) of the UUV dedicated to the energy section affects the mission duration, as shown in Fig. 11. In doing this analysis, the neutral buoyancy of the system is realized; $W_{total}$ and $V_{total}$ in Eqs. (22) and (23) are known and the mission duration is found by solving the system of equations. The mission length increases with increasing the length of the energy section

dedicated to fuel storage, as would be expected. Several hydrogen storage technologies are compared in Fig. 11. Use of a hybrid fuel cell/battery system always gives longer mission length than using a purely Li-ion battery system, supporting the decision to use a hybrid system. For the hybrid fuel cell/battery system, supplying hydrogen using $NH_3BH_3$ storage is predicted to give the longest mission length due to the encouraging estimation for its gravimetric and volumetric $H_2$ density. This strongly supports the demand of hydrogen storage with both high gravimetric and volumetric density especially in applications (e.g. transportation) where both the weight and space are constraints. Nevertheless, one has to recognize that the impressive figures for $NH_3BH_3$ used in this analysis are based on continued progress in delivering a high performance hydrogen delivery system. Furthermore, several methods exist for releasing hydrogen from $NH_3BH_3$, such as thermal decomposition and hydrolysis with various catalysts. These release processes may require elevated temperatures, or introduce other reactor design requirements, which could raise issues of system complexity and energy efficiency. Therefore, it is appropriate to recommend liquid hydrogen as the best hydrogen storage technique currently available for this UUV application, whilst recognising the potential longer term benefit of the $NH_3BH_3$ option.

## 4. Conclusions

We have demonstrated a sizing-design methodology for designing hybrid fuel cell power systems. The criteria for the choice of fuel cell technology, battery or supercapacitor technology, hydrogen storage method and means of oxygen supply have been examined.

We have also demonstrated the application of the sizing-design methodology to a light-weight UUV. The analysis is focused on the mass, size, and the energy balance of the system components. The selected hybrid system comprises a lithium-ion battery, a polymer electrolyte fuel cell, a liquid oxygen tank, a hydrogen tank and other balance-of-plant components. The hybrid fuel cell/battery system is observed to have significant advantages over a purely battery powered design in terms of extended mission duration. Hydrogen storage constitutes a large part of the mass and volume of the energy system. Compact hydrogen storage with high energy density (in both gravimetric and volumetric terms) is beneficial, which enables the UUV to have a longer mission length. Shortening the mission length enables the use of currently available but less compact hydrogen storage methods, such as compressed hydrogen. Hydrogen storage in the form of $NH_3BH_3$ has been identified to have a particularly high storage density; however, the practicalities of using such a system have not been assessed since there is no commercial product currently available. Among the commercially available techniques, liquid hydrogen stored in cryogenic tanks provides the most promising performance.

## Acknowledgements

The work reported in this paper was funded by the Systems Engineering for Autonomous Systems (SEAS) Defence Technology Centre established by the UK Ministry of Defence.

## References

[1] C. Bernay, M. Marchand, M. Cassir, J. Power Sources 108 (2002) 139–152.
[2] M. Granovskii, I. Dincer, M.A. Rosen, J. Power Sources 159 (2006) 1186–1193.
[3] R.M. Moore, K.H. Hauer, S. Ramaswamy, J.M. Cunningham, J. Power Sources 159 (2006) 1214–1230.
[4] M. Kim, Y.J. Sohn, W.Y. Lee, C.S. Kim, J. Power Sources 178 (2008) 706–710.
[5] H. Yun, Y. Zhao, Z. Sun, G. Wan, J. Power Sources 180 (2008) 821–829.
[6] K.S. Jeong, B.S. Oh, J. Power Sources 105 (2002) 58–65.
[7] P. Rodatz, G. Paganelli, A. Sciarretta, L. Guzzella, Control Eng. Pract. 13 (2005) 41–53.
[8] Y. Jia, H. Wang, M. Ouyang, J. Power Sources 155 (2006) 319–324.
[9] M.-J. Kim, H. Peng, J. Power Sources 165 (2007) 819–832.
[10] R.K. Ahluwalia, X. Wang, J. Power Sources 139 (2005) 152–164.
[11] N. Lapeña-Rey, J. Mosquera, E. Bataller, F. Ortí, C. Dudfield, A. Orsillo, J. Power Sources 181 (2008) 353–362.
[12] P. Aguiar, D.J.L. Brett, N.P. Brandon, Int. J. Hydrogen Energy 33 (2008) 7214–7223.
[13] G. Griffiths, D. Reece, P. Blackmore, M. Lain, S. Mitchell, J. Jamieson, Proceedings of 14th Unmanned Untethered Submersible Technology, Durham, 2005.
[14] M.T. Gencoglu, Z. Ural, Int. J. Hydrogen Energy (2008) 1–7.
[15] L.P. Jarvis, T.B. Atwater, P.J. Cygan, J. Power Sources 79 (1999) 60–63.
[16] P.B. Jones, J.B. Lakeman, G.O. Mepsted, J.M. Moore, J. Power Sources 80 (1999) 242–247.
[17] T. Yalcinoz, M.S. Alam, Int. J. Hydrogen Energy 33 (2008) 1932–1940.
[18] Y.D. Zhan, Y.G. Guo, J.G. Zhu, H. Wang, J. Power Sources 179 (2008) 745–753.
[19] Z.H. Jiang, L.J. Gao, M.J. Blackwelder, R.A. Dougal, J. Power Sources 130 (2004) 163–171.
[20] J. Larminie, J. Lowry, Electric Vehicle Technology: Explained, John Wiley & Sons Ltd., UK, 2003.
[21] V. Paladini, T. Donateo, A.d. Risi, D. Laforgia, Energy Convers. Manage. 48 (2007) 3001–3008.
[22] W. Henson, J. Power Sources 179 (2008) 417–423.
[23] Woodbank Communications Ltd., http://www.mpoweruk.com/performance.htm, accessed on 01/12/2009.
[24] D.J.L. Brett, P. Aguiar, N.P. Brandon, R.N. Bull, R.C. Galloway, G.W. Hayes, K. Lillie, C. Mellors, C. Smith, Tilley, J. Power Sources 157 (2006) 782–798.
[25] Cobasys, http://www.cobasys.com/pdf/faq/faq.html, accessed on 01/12/2009.
[26] Sony Group, http://www.sony.net/SonyInfo/News/Press/200908/09-083E/index.html, accessed on 01/12/2009.
[27] M. Conte, P.P. Prosini, S. Passerini, Mater. Sci. Eng. B 108 (2004) 2–8.
[28] Ø. Hasvold, N.J. Størkersen, S. Forseth, T. Lian, J. Power Sources 162 (2006) 935–942.
[29] L.T. Lam, R. Louey, J. Power Sources 158 (2006) 1140–1148.
[30] T.R. Crompton, Battery Reference Book, Butterworth-Heinrmann Ltd., Oxford, 1995.
[31] D. Berndt, Maintenance-free Batteries: Based on Aqueous Electrolyte Lead-acid, Nickel/cadmium, Nickel/metal hydride: A Handbook of Battery Technology Baldock, Research Studies Press Ltd., Hertfordshire, England, 2003.
[32] S.G. Chalk, J.F. Miller, J. Power Sources 159 (2006) 73–80.
[33] F. Barbir, PEM Fuel Cells: Theory and Practice, Elsevier Academic Press, USA, 2005.
[34] P. Fontela, A. Soria, J. Mielgo, J.F. Sierra, J.d. Blas, L. Gauchia, J.M. Martínez, J. Power Sources 169 (2007) 184–193.
[35] R.v. Helmolt, U. Eberle, J. Power Sources 165 (2007) 833–843.
[36] K. Haraldsson, P. Alvfors, J. Power Sources 145 (2005) 298–306.
[37] B. Lin, J. Power Sources 86 (2000) 202–213.
[38] D.J.L. Brett, A. Atkinson, N.P. Brandon, S. Skinner, Chem. Soc. Rev. 37 (2008) 1568–1578.
[39] D.J.L. Brett, P. Aguiar, N.P. Brandon, J. Power Sources 163 (2006) 514–522.
[40] P. Aguiar, D.J.L. Brett, N.P. Brandon, J. Power Sources 171 (2007) 186–197.
[41] A. Hawkes, I. Staffell, D. Brett, N.P. Brandon, Energy Environ. Sci. 2 (2009) 729–744.
[42] E.D. Geeter, M. Mangan, S. Spaepen, W. Stinissen, G. Vennekens, J. Power Sources 80 (1999) 207–212.
[43] W. Luo, J. Wang, K. Stewart, M. Clift, K. Gross, J. Alloys Compd. 446/447 (2007) 336–341.
[44] J. Yang, et al., J. Alloys Compd. 446/447 (2007) 345–349.
[45] U.B. Demirci, O. Akdim, P. Miele, Int. J. Hydrogen Energy 34 (2009) 2638–2645.
[46] J.F. Mao, X.B. Yu, Z.P. Guo, H.K. Liu, Z. Wu, J. Ni, J. Alloys Compd. 479 (2009) 619–623.
[47] A. Züttel, Mater. Today 6 (2003) 24–33.
[48] A. Burke, M. Gardiner, Hydrogen Storage Options: Technologies and Comparisons for Light-duty Vehicle Applications, University of California-Davis, USA, 2005.
[49] C.L. Aardahl, S.D. Rassat, Int. J. Hydrogen Energy 34 (2009) 6676–6683.
[50] Ø. Hasvold, K.H. Johansen, O. Mollestad, S. Forseth, N. Størkersen, J. Power Sources 80 (1999) 254–260.
[51] M.G. Medeiros, E.G. Dow, J. Power Sources 80 (1999) 78–82.
[52] M.G. Medeiros, R.R. Bessette, C.M. Deschenes, C.J. Patrissi, L.G. Carreiro, S.P. Tucker, D.W. Atwater, J. Power Sources 136 (2004) 226–231.
[53] J.B. Lakeman, A. Rose, K.D. Pointon, D.J. Browning, K.V. Lovell, S.C. Waring, J.A. Horsfall, J. Power Sources 162 (2006) 765–772.
[54] A.A. Burke, L.G. Carreiro, E.S. Greene, J. Power Sources 176 (2008) 299–305.
[55] A.A. Burke, L.G. Carreiro, J. Power Sources 158 (2006) 428–435.
[56] T. Aoki, T. Murashima, S. Tsukioka, H. Yoshida, T. Hyakudome, A. Hashimoto, K. Hashizaki, T. Tani, K. Yokoyama, 10th FCDIC Fuel Cell Symposium Proceedings, 2003, pp. 90–95.
[57] T. Fulton, Online Information for the Defence Community, http://www.dtic.mil/ndia/2005umv_auv/tuesday/fulton.pdf, accessed on 11/11/2009.
[58] E.J. Carlson, P. Kopf, J. Sinha, S. Sriramulu, Y. Yang, Cost analysis of PEM fuel cell systems for transportation, Report of National Renewable Energy Laboratory, Massachusetts, 2007.
[59] S. Willen, Proceedings of 7th International Symposium on Unmanned Untethered Submersible Technology, University of New Hampshire, 1991, pp. 89–103.